Electronic structure and magnetism of the Hund's insulator CrI_3

Tianye Yu, Rui Liu, Huican Mao, Xiaobo Ma, Guangwei Wang, Zhihong Yuan, Pengyu Zheng, Yiran Peng, and Zhiping Yin*
Department of Physics and Center for Advanced Quantum Studies, Beijing Normal University, Beijing 100875, China

(Received 8 November 2021; revised 21 March 2022; accepted 4 April 2022; published 15 April 2022)

CrI_3 is a two-dimensional ferromagnetic (FM) van der Waals material with a charge gap of 1.1–1.2 eV. In this paper, the electronic structure and magnetism of CrI_3 are investigated by using density functional theory and dynamical mean-field theory. Our calculations successfully reproduce a charge gap of ∼1.1 eV in the paramagnetic (PM) state when a Hund's coupling $J_H = 0.7$ eV is included with an onsite Hubbard $U = 5$ eV. In contrast, with a large U value of 8 eV and negligible Hund's coupling J_H, CrI_3 is predicted to be a moderately correlated metal in the PM state. We conclude that CrI_3 is a Mott-Hund's insulator due to the half-filled configuration of the Cr 3d t_{2g} orbitals. The Cr 3d e_g orbitals are occupied by ∼1 electron, which leads to strong valence fluctuations so that the Cr 3d orbitals cannot be described by a single state. Moreover, at finite temperature, the calculated ordered static magnetic moment in the FM state is significantly larger in the $R\bar{3}$ phase than in the $C2/m$ phase. This observation indicates that the structural phase transition from the $C2/m$ phase to the $R\bar{3}$ phase with decreasing temperature is driven by FM spin fluctuations.

DOI: 10.1103/PhysRevB.105.165127

I. INTRODUCTION

Since the discovery of graphene [1–3], the field of two-dimensional (2D) materials has attracted widespread attention because of their outstanding mechanical, optical, electrical properties, etc. [4–9]. CrI_3 is another 2D van der Waals material. Recently, Huang *et al.* [10] reported that, with Curie temperatures (T_c) as high as 45 K, ferromagnetism can be retained in monolayer CrI_3, which is mainly due to the breaking of the Mermin-Wagner theorem [11], where strong magnetic anisotropy counteracts thermal fluctuations, thus stabilizing the long-range magnetic order.

In CrI_3, one Cr ion lies at the center of the octahedron formed by six neighboring iodine ions, and each monolayer is made up of edge-shared CrI_6 octahedrons [12]. Upon cooling, CrI_3 undergoes a structural phase transition at ∼220 K from a high-temperature (HT) monoclinic phase with space group $C2/m$ to a low-temperature (LT) rhombohedral phase $R\bar{3}$ [12–14]. McGuire *et al.* [12] reported that CrI_3 is an insulating ferromagnet with a T_c of 61 K, and every Cr ion has a static magnetic moment of ∼3.1 μ_B aligning vertically to each monolayer. The bandgap determined by optical experiments is 1.1–1.2 eV [15–17] and is independent of temperature [16]. Interestingly, the magnetism of CrI_3 is strongly layer dependent: both monolayer and bulk CrI_3 are ferromagnetic (FM) [12], while the bilayer exhibits antiferromagnetic (AFM) interlayer coupling [10,16,18–22]. First-principles calculations demonstrated that the AFM coupling between the bilayers comes from a different stacking order with the $C2/m$ rather than the $R\bar{3}$ space group symmetry [23], which is consistent with other research results [24,25]. Furthermore, when different values of the Hubbard U are applied in first-principles calculations, different magnetic states, including AFM and FM states, may be the ground state [23]. Recently, Zhang *et al.* [26] pointed out that there is a close relationship between electronic correlations and magnetism in another van der Waals crystal $CrSiTe_3$. Therefore, it is crucial to appropriately treat the strong correlation among Cr 3d electrons to understand the magnetism of this material.

Although the insulating phase in the FM state has been investigated within the generalized gradient approximation (GGA) and GGA + U schemes for CrI_3 [27–30], little research on the insulating phase in the paramagnetic (PM) state has been done. Recently, Craco *et al.* [31,32] reproduced the PM Mott insulating state through density functional theory (DFT) in combination with dynamical mean-field theory (DMFT). Comparing the results obtained by DFT + DMFT calculations with different values of U, they concluded that orbital-selective reconstruction plays an important role in this material. In addition, McNally *et al.* [33] reported that Hund's coupling J_H determines the charge gap of transition metal materials with half-filled 3d orbitals, such as LaMnPO. The octahedral environment of Cr in CrI_3 leads to a large crystal field splitting between the Cr 3d t_{2g} and e_g orbitals and results in half-filled Cr 3d t_{2g} orbitals. Despite the similarity of electron filling between CrI_3 and LaMnPO, the role of J_H in the charge gap of CrI_3 remains unclear. Furthermore, the driving force of the structural phase transition upon cooling has not been explored. To answer these questions, we adopted the DFT + DMFT approach to address the strongly correlated effect of Cr^{3+} 3d orbitals and analyzed the electronic structure, atomic histogram, and magnetism of CrI_3.

II. COMPUTATIONAL DETAILS

In this paper, we adopt the experimental lattice constants and atomic positions [12] in all calculations. To consider electronic correlation effects, we use the fully charge self-consistent combination of DFT and DMFT (DFT + DMFT)

*yinzhiping@bnu.edu.cn

[34,35] to theoretically study this material in the PM and FM states. For the DFT part, we use the GGA-PBE exchange correlation functional [36] implemented in the WIEN2K all-electron DFT package [37]. Brillouin zone integrations are performed on a $17 \times 17 \times 17$ mesh for the LT phase and an $18 \times 14 \times 18$ mesh for the HT phase. The atomic spheres R_{MT} are 2.49 and 2.50 Bohr for Cr and I, respectively, and the plane-wave cutoff $K_{\max}$ is given by $R_{\mathrm{MT}}K_{\max} = 9.0$. To understand the origin of the charge gap in the PM state, both $U = 8\,\mathrm{eV}$, $J_{\mathrm{H}} = 0\,\mathrm{eV}$ and $U = 5\,\mathrm{eV}$, $J_{\mathrm{H}} = 0.7\,\mathrm{eV}$ are used in the calculations. The impurity problem in the DFT + DMFT calculation is solved by the continuous time quantum Monte Carlo (CTQMC) method with exact double counting, as proposed in Ref. [38]. In the DMFT impurity solver, we adopt the density-density form of Coulomb repulsion, which speeds up calculation considerably. We break the symmetry between spin up and spin down in the self-energy to simulate the FM order of CrI_3. To reduce the sign problem in the CTQMC, we use the local axis where the new x and y axes are nearly aligned with the in-plane Cr-I bond direction in an octahedral environment. After achieving the desired accuracy, we perform analytical continuation using the maximum entropy method [35] to obtain the self-energy on the real axis and then calculate the electronic structure. We have checked that spin-orbit coupling affects little on our main findings, and we show the band structures obtained with the inclusion of spin-orbit coupling in Fig. S2 in the Supplemental Material [39]. For simplicity, we report only the results calculated without spin-orbit coupling in the main paper.

III. RESULTS AND DISCUSSION

A. Band structure and density of states

The electronic band structures of CrI_3 with the LT and HT crystal structures are calculated by the DFT + DMFT method at $T = 50\,\mathrm{K}$ in the PM state [Figs. 1(a), 1(b), 1(e), and 1(f)] and FM state [Figs. 1(c), 1(d), 1(g), and 1(h)], respectively. Figure 2 presents the corresponding density of states (DOS) of Fig. 1. Since the band structures and DOSs of the HT and LT structures are similar, we focus on the results of the LT structure. The band structure and DOS shown in Figs. 1(a) and 2(a) are obtained by a large Hubbard $U = 8\,\mathrm{eV}$ and a vanishing Hund's coupling $J_{\mathrm{H}} = 0\,\mathrm{eV}$. According to experimental results, CrI_3 is an insulator even above T_c [17,40]. However, the band structure shown in Fig. 1(a) shows metallicity instead of a charge gap in the PM state. The metallicity is characterized by a nonzero DOS around the Fermi level [Fig. 2(a)], which is dominated by contributions from the Cr $3d$ t_{2g} and I $5p$ orbitals. This disagreement between the calculations and experiments illustrates the possibility that CrI_3 is not a conventional Mott-Hubbard insulator since a large Hubbard $U = 8\,\mathrm{eV}$ alone cannot open the charge gap.

In previous DMFT calculations, the role of Hund's coupling J_{H} is highlighted for electronic correlations not only in metallic [41–45] but also insulating systems [33]. To consider J_{H}, the other calculations in Figs. 1 and 2 adopt a more realistic combination of $U = 5\,\mathrm{eV}$ and $J_{\mathrm{H}} = 0.7\,\mathrm{eV}$, with which the experimental charge gap of CrI_3 and the magnetic moment of Cr are very well reproduced. As shown in Figs. 1(b) and 2(b),

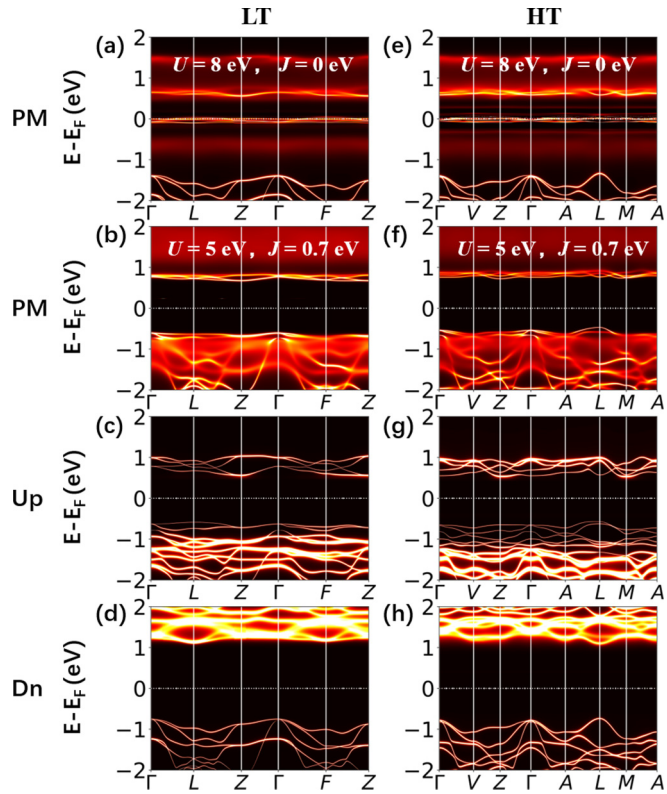

FIG. 1. The density functional theory (DFT) + dynamical mean-field theory (DMFT) electronic band structures at $T = 50\,\mathrm{K}$ with a Hubbard $U = 5\,\mathrm{eV}$ and Hund's coupling $J_{\mathrm{H}} = 0.7\,\mathrm{eV}$, except in (a) and (e), where $U = 8\,\mathrm{eV}$ and $J_{\mathrm{H}} = 0\,\mathrm{eV}$ were used. Left (right) column is for low-temperature (LT) [high-temperature (HT)] structure. The first two rows are for the paramagnetic (PM) state, and the last two rows are for the ferromagnetic (FM) state. "Up" and "Dn" denote spin up and spin down, respectively.

when Hund's coupling $J_{\mathrm{H}} = 0.7\,\mathrm{eV}$ and Hubbard $U = 5\,\mathrm{eV}$ are used, CrI_3 exhibits insulating characteristics with a charge gap of $\sim$1.1 eV in the PM state, which is in excellent agreement with the experimental value [15,46]. It demonstrates that J_{H} plays an important role in opening the charge gap. Similarly, Chen *et al.* [47] reproduced the charge gap of CrI_3 in the PM state by applying the disordered local moment picture and proved the importance of intra-atomic exchange interaction. We also find that a similar charge gap exists in both majority-spin [Fig. 1(c)] and minority-spin electronic bands [Fig. 1(d)] for CrI_3 in the FM state when $U = 5\,\mathrm{eV}$ and $J_{\mathrm{H}} = 0.7\,\mathrm{eV}$ are used, in accordance with previous spin-polarized DFT calculations and experiments [12,27].

In CrI_3, the Cr atom has the nominal valence Cr^{3+} ($3d^3$ electronic state) with three electrons occupying the $3d$ shell, which is different from the calculated Cr $3d$ orbital occupation number ($\sim$4) with $\sim$3 electrons in the t_{2g} orbitals and $\sim$1 electron in the e_g orbitals (Table I). This difference in the orbital occupation number of Cr ions between nominal valence and DFT + DMFT calculations comes from the strong hybridization between Cr $3d$ e_g and I $5p$ orbitals $\sim$3 eV below the Fermi level, as shown in Fig. 2. Furthermore, we find that the static magnetic moment of Cr in the FM state is mainly from the t_{2g} orbitals due to its nearly complete occupation in the

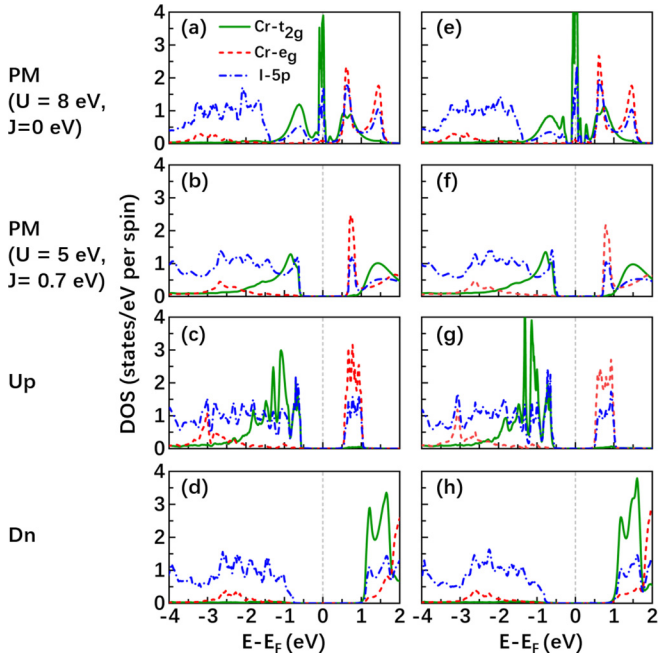

FIG. 2. The density functional theory (DFT) + dynamical mean-field theory (DMFT) electronic density of states per unit cell at $T = 50\,\mathrm{K}$ with a Hubbard $U = 5\,\mathrm{eV}$ and Hund's coupling $J_\mathrm{H} = 0.7\,\mathrm{eV}$, except in (a) and (e), where $U = 8\,\mathrm{eV}$ and $J_\mathrm{H} = 0\,\mathrm{eV}$ were used. Left (right) column is for low-temperature (LT) [high-temperature (HT)] structure. The first two rows are for the paramagnetic (PM) state, and the last two rows are for the ferromagnetic (FM) state. "Up" and "Dn" denote spin up and spin down, respectively.

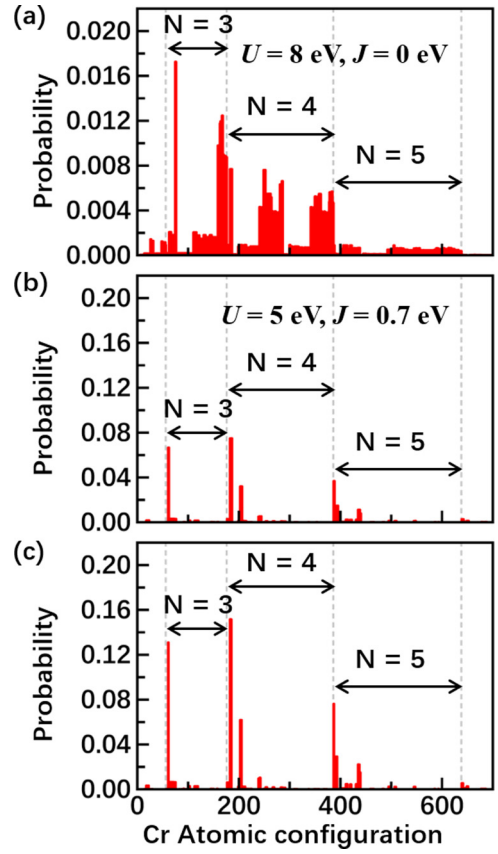

FIG. 3. Density functional theory (DFT) + dynamical mean-field theory (DMFT) calculated atomic histogram of Cr $3d$ orbitals in CrI_3 with the low-temperature (LT) structure: (a) paramagnetic (PM) state with $U = 8\,\mathrm{eV}$ and $J_\mathrm{H} = 0\,\mathrm{eV}$. (b) PM state and (c) ferromagnetic (FM) state with $U = 5\,\mathrm{eV}$ and $J_\mathrm{H} = 0.7\,\mathrm{eV}$. The probability scale of (a) is only one tenth of (b) and (c). The states with occupation number exceeding five are not shown due to their negligible probabilities.

majority-spin channel with 2.84 electrons and nearly empty occupation in the minority-spin channel with 0.11 electrons, as shown in the calculated DOSs [Figs. 2(c) and 2(d)] and averaged orbital occupation numbers (Table I).

For an isolated atom, the first of Hund's empirical rules states that a maximum total spin S minimizes the total energy. This rule also works for the Cr atom in CrI_3 solid where the ~3 electrons occupying the Cr $3d$ t_{2g} orbitals in CrI_3 tend to have parallel spins and different angular quantum numbers. It is not favorable for electrons to hop out of or into the Cr $3d$ t_{2g} orbitals, which reduces S and suffers additional energy penalty. As a result, the hopping from and to the Cr $3d$ t_{2g} orbitals is forbidden, and a charge gap opens. We conclude that CrI_3 is not a conventional Mott-Hubbard insulator but a Mott-Hund's insulator. As shown in Table SIV in the Supplemental Material [39], this conclusion is also supported by the fact that the Cr static magnetic moment in the FM state is far more sensitive to J_H than U.

TABLE I. The CTQMC averaged orbital occupation of Cr $3d$ orbitals from the charge self-consistent DFT + DMFT calculations in the PM and FM states with LT and HT structures at $T = 50\,\mathrm{K}$. "Up" and "dn" denote spin-up and spin-down electrons, respectively.

	Orbital occupation						
	tot	t_{2g}	e_g	t_{2g} up	t_{2g} dn	e_g up	e_g dn
LT PM	4.08	2.96	1.13	1.48	1.48	0.57	0.57
LT FM	4.09	2.95	1.13	2.84	0.11	0.76	0.37
HT PM	4.08	2.96	1.13	1.48	1.48	0.57	0.57
HT FM	4.09	2.95	1.13	2.81	0.14	0.75	0.38

B. Characteristics of Hund's insulators: Atomic histogram

Figure 3 presents the Cr $3d$ atomic histogram of the LT structure at 50 K in the PM state with $U = 8\,\mathrm{eV}$, $J_\mathrm{H} = 0\,\mathrm{eV}$ [Fig. 3(a)] and $U = 5\,\mathrm{eV}$, $J_\mathrm{H} = 0.7\,\mathrm{eV}$ [Fig. 3(b)], and in the FM state with $U = 5\,\mathrm{eV}$, $J_\mathrm{H} = 0.7\,\mathrm{eV}$ [Fig. 3(c)]. The atomic histograms of the LT and HT structures at 50 K are almost the same; hence, the histogram of the HT structure is not shown. Within the DFT + DMFT scheme, each Cr impurity has 1024 $3d$ states. The atomic histogram refers to the probability of finding a Cr impurity in each atomic state. We note that only those states occupied by $N = 3$, 4, and 5 electrons have considerable probabilities; thus, the states with larger orbital occupation number ($N > 5$) are not presented in Fig. 3. For the states with the same occupation number N, we arrange the states in descending order in accordance with their $|S_z|$ values. As shown in Fig. 3(b), when using Hund's coupling $J_\mathrm{H} = 0.7\,\mathrm{eV}$, only high-spin states have large

probabilities. For comparison, when a negligible Hund's coupling $J_H = 0$ eV is used, the probabilities for the high-spin states decrease drastically, while some low-spin states gain comparable probabilities, as shown in Fig. 3(a). It demonstrates that Hund's coupling J_H tends to align the spins of the Cr 3*d* electrons in parallel.

We now focus on the histograms of the PM and FM states with realistic Hund's coupling $J_H = 0.7$ eV. As shown in Figs. 3(b) and 3(c), in both the PM and the FM states, the high-spin states with occupation numbers $N = 3$, 4, and 5 have the highest probabilities of being occupied, suggesting that there are strong valence fluctuations in CrI_3, which share similarities with the histogram of Hund's metals (such as iron pnictides [45]), whereas the valence fluctuations are stronger than those previously reported in the Hund's insulator LaMnPO [33,48]. To trace the origin of the strong valence fluctuations in CrI_3, we check all the 3*d* states (1024 states) and sort them according to the configuration of the t_{2g} orbitals (explained in detail in the Supplemental Material [39]). As shown in Table SIII in the Supplemental Material [39], the electrons in the t_{2g} orbitals tend to have parallel spins, whereas the electrons of e_g orbitals are arranged randomly. Therefore, Cr 3*d* e_g orbitals are responsible for the strong valence fluctuations in CrI_3.

The strong fluctuations in the e_g orbitals give rise to a negligible spin moment of the e_g electrons in the FM state. The occupation number of Cr 3*d* orbitals calculated within the DFT + DMFT scheme is ∼4 (Table I), out of which three are for t_{2g} orbitals and one is for e_g orbitals. Therefore, the DFT + DMFT calculated static magnetic moment of ∼3.1 μ_B comes mainly from the t_{2g} orbitals due to Hund's rule and is in excellent agreement with the experimental value of ∼3.1 μ_B at low temperature [12].

C. Magnetism and structural phase transition at finite temperature

Figure 4 presents the Cr magnetic moment vs T obtained by the DFT + DMFT calculations for both the LT and HT structures. The fluctuating magnetic moment is nearly independent of temperature or structure (∼3.1 μ_B per Cr for the LT and HT structures at both 50 and 160 K), so only the fluctuating magnetic moments of the LT structure at various temperatures are shown for clarity. The fluctuating magnetic moment is calculated according to the formula $\langle m_z \rangle = 2\sum_i P_i |S_z|_i$, where i is the index of the 1024 atomic states, and P_i and $|S_z|_i$ are the corresponding probability and absolute value of the total spin, respectively. Consequently, the value of the fluctuating magnetic moment is the upper limit of the static magnetic moment in the magnetically ordered states. The fluctuating magnetic moment is equal to the static magnetic moment of the FM order only if quantum fluctuations vanish. As shown in Fig. 4, the fluctuating magnetic moment hardly changes with decreasing temperature. It is expected that the fluctuating magnetic moment is ∼3.1 μ_B at very low temperatures. At 50 K, the calculated static magnetic moment in the FM state is already very close to the fluctuating magnetic moment, suggesting that the FM static magnetic moment is ∼3.1 μ_B at 2 K, which agrees well with the experimental value [12].

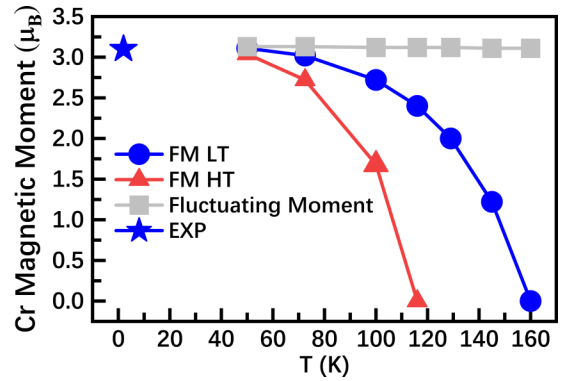

FIG. 4. The density functional theory (DFT) + dynamical mean-field theory (DMFT) calculated magnetic moments of Cr at different temperatures for both the low-temperature (LT) and high-temperature (HT) structures. The blue circle and red triangle represent the values of the ferromagnetic static magnetic moments of the LT and HT structures, respectively. The calculated fluctuating magnetic moment of the LT structure is shown as a gray square. The experimentally determined static magnetic moment [12] at $T = 2$ K is shown as a blue star.

Our DFT calculated static magnetic moments of the LT and HT structures in the FM state are the same, ∼3.0μ_B per Cr, which is consistent with previous calculated results [12]. In contrast, as shown in Fig. 5, the DFT + DMFT calculated FM static magnetic moments of the LT and HT structures exhibit clear differences at finite temperatures, where the static magnetic moment of the HT structure drops much faster than that of the LT structure with increasing temperature. As a result, the calculated Curie temperature T_c (the temperature corresponding to the disappearance of the static magnetic moment) of the HT structure is ∼116 K, while the static magnetic moment of the LT structure remains at ∼2.4 μ_B per Cr at the same temperature. Therefore, we conclude that the structural

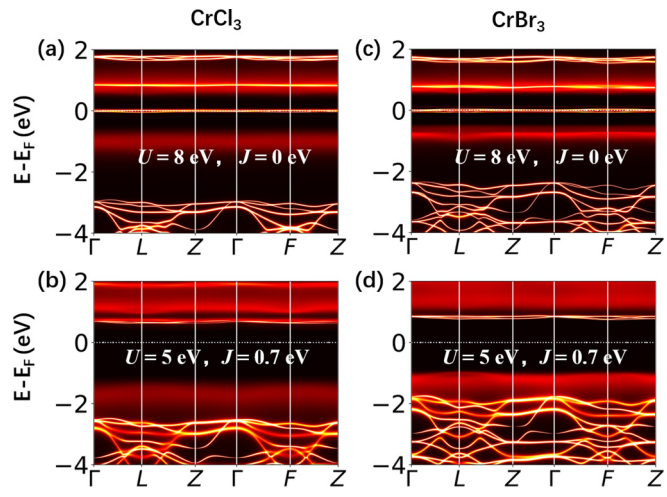

FIG. 5. The density functional theory (DFT) + dynamical mean-field theory (DMFT) calculated electronic band structures at (a) and (c) $T = 50$ K with $U = 8$ eV, $J_H = 0$ eV and (b) and (d) $U = 5$ eV, $J_H = 0.7$ eV of (a) and (b) $CrCl_3$ and (c) and (d) $CrBr_3$ in the paramagnetic state. Both $CrCl_3$ and $CrBr_3$ are in the $R\bar{3}$ phase.

differences between the HT and LT structures originating from stacking pattern have little effect on the fluctuating magnetic moment but are essential to the static magnetic moment in the FM state, especially at high temperatures. We note that the T_c calculated from the DFT + DMFT method is generally higher than the experimentally determined value ($T_c \sim 61$ K), which is not surprising since DFT + DMFT calculations neglect spatial fluctuations of the magnetic order.

Based on the Heisenberg model $H = -J \sum_{l,\delta} \hat{s}_l \cdot \hat{s}_{l+\delta}$, we can estimate the magnetic coupling energy of systems with different magnetic orders. In CrI_3, the structural differences between the LT and HT phases mainly originate from different stacking orders, which indicates that there are some differences in the interlayer magnetic coupling parameters J_2, whereas the intralayer coupling parameters J_1 are almost identical for the two phases. Previous calculations [28] and experiments [49] demonstrate that the magnetic coupling parameter J_1 is much larger than J_2 in CrI_3 and two other chromium halides including $CrCl_3$ [50] and $CrBr_3$ [51–53] by means of spin-wave analysis. Therefore, the interlayer magnetic coupling is negligible, which shows that the magnetic coupling energy of the Heisenberg model depends chiefly on the intralayer coupling J_1. In Fig. 4, we find that the FM Cr static magnetic moment of the LT phase is always larger than that of the HT phase at the same temperature. According to the Heisenberg model, the LT structure is more stable with lower energy because it has a larger static magnetic moment and almost the same nearest-neighbor exchange interaction parameter as the HT phase. For example, the magnetic coupling energy of the LT phase is ~2.6 times lower than that of the HT phase at 100 K. Regarding the structural phase transition from the HT to the LT phase with decreasing temperature in CrI_3, the magnetic coupling energy greatly contributes to the difference in the total energy between the two phases. Therefore, we propose that the structural phase transition from the HT to the LT phase is driven by FM spin fluctuations.

D. Two other Hund's insulators: $CrCl_3$ and $CrBr_3$

In addition to CrI_3, we have carried out DFT + DMFT calculations of the electronic structures of two other chromium halides $CrCl_3$ and $CrBr_3$ in the $R\bar{3}$ phases using both $U = 8$ eV, $J_H = 0$ eV and $U = 5$ eV, $J_H = 0.7$ eV. The lattice constants and atomic positions of $CrCl_3$ are taken from Ref. [54], while the lattice constants of $CrBr_3$ are taken from Ref. [55]. The atomic positions of $CrBr_3$ are not provided in Ref. [55], hence are fully optimized using the Vienna *Ab initio* Simulation Package (VASP) [56] until all the force components become <0.04 eV/Å, which is consistent with previous calculations [31,32]. We come to the same conclusion that Hund's coupling is decisive for the charge gap in the PM state in both $CrCl_3$ and $CrBr_3$. As shown in Figs. 5(a) and 5(c), despite a large U value of 8 eV, there are several bands crossing the Fermi level when Hund's coupling is absent, i.e., $J_H = 0$. In contrast, there are charge gaps in the band structures obtained by using $U = 5$ eV and $J_H = 0.7$ eV, as shown in Figs. 5(b) and 5(d). Consequently, our conclusion that CrI_3 is a Mott-Hund's insulator rather than a Mott-Hubbard insulator also applies to $CrCl_3$ and $CrBr_3$. In Fig. 6, we present a comparison of the DFT + DMFT calculated DOSs of $CrCl_3$, $CrBr_3$, and CrI_3 obtained using $U = 5$ eV and $J_H = 0.7$ eV in the PM state. From $CrCl_3$ to CrI_3, we find that the bandgap gets smaller, and the peaks of DOSs of the Cr t_{2g} and e_g orbitals above the Fermi level get broader. Below the Fermi level, the energy region of the Cr t_{2g} orbitals hybridizing with the halogen element p orbitals gets closer to the Fermi level, as shown in Figs. 6(a)–6(c).

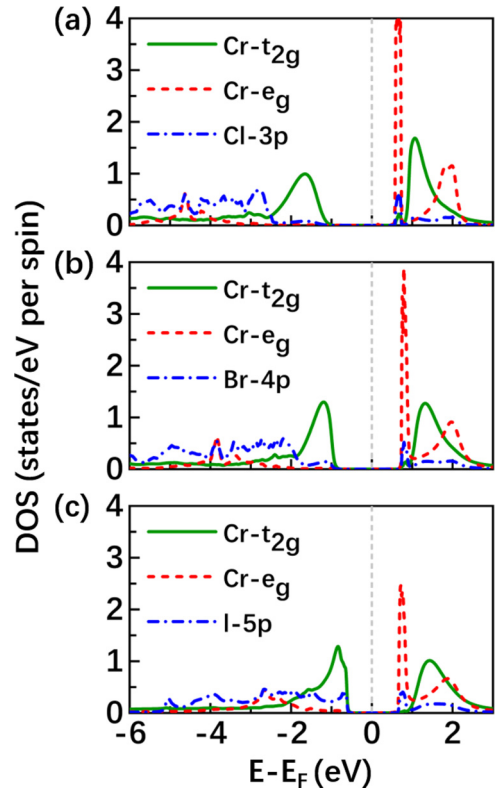

FIG. 6. The density functional theory (DFT) + dynamical mean-field theory (DMFT) calculated electronic density of states per unit cell in the paramagnetic (PM) state at $T = 50$ K with $U = 5$ eV, $J_H = 0.7$ eV of (a) $CrCl_3$, (b) $CrBr_3$, and (c) CrI_3 in the $R\bar{3}$ phase.

IV. CONCLUSIONS

Our DFT + DMFT calculations indicate that CrI_3 is a Mott-Hund's insulator rather than a conventional Mott-Hubbard insulator. Including a realistic Hund's coupling $J_H \sim 0.7$ eV is essential to open a charge gap of ~1.1 eV in the PM state. This conclusion also applies to other chromium halides including $CrCl_3$ and $CrBr_3$. By analyzing the atomic histogram of the Cr $3d$ shell, we find that the strong valence fluctuations in CrI_3 come mainly from Cr e_g orbitals, unlike the valence fluctuations in the previously observed Mott-Hund's insulator LaMnPO, where all the $3d$ orbitals are responsible for the valence fluctuations [33]. The calculated static magnetic moment of Cr ions in the FM state in the LT $R\bar{3}$ phase is larger than that in the HT $C2/m$ phase at the same temperature. Therefore, the $R\bar{3}$ phase is more stable with a lower magnetic coupling energy at low temperature, which suggests that the driving force of the structural phase transition from the $C2/m$ to the $R\bar{3}$ phase upon cooling is FM spin fluctuations.

ACKNOWLEDGMENTS

This paper was supported by the National Natural Science Foundation of China (Grants No. 12074041 and No. 11674030), the Foundation of the National Key Laboratory of Shock Wave and Detonation Physics (Grant No. 6142A03191005), the National Key Research and Development Program of China through Contract No. 2016YFA0302300, and the startup funding of Beijing Normal University. The calculations were carried out with the high-performance computing cluster of Beijing Normal University in Zhuhai.

[1] Y. Zhang, Y.-W. Tan, H. L. Stormer, and P. Kim, Nature (London) **438**, 201 (2005).

[2] K. S. Novoselov, A. K. Geim, S. V. Morozov, D. Jiang, M. I. Katsnelson, I. Grigorieva, S. Dubonos, and A. A. Firsov, Nature (London) **438**, 197 (2005).

[3] K. S. Novoselov, A. K. Geim, S. V. Morozov, D. Jiang, Y. Zhang, S. V. Dubonos, I. V. Grigorieva, and A. A. Firsov, Science **306**, 666 (2004).

[4] K. S. Novoselov, Rev. Mod. Phys. **83**, 837 (2011).

[5] A. H. Castro Neto, F. Guinea, N. M. R. Peres, K. S. Novoselov, and A. K. Geim, Rev. Mod. Phys. **81**, 109 (2009).

[6] C.-T. Toh, H. Zhang, J. Lin, A. S. Mayorov, Y.-P. Wang, C. M. Orofeo, D. B. Ferry, H. Andersen, N. Kakenov, Z. Guo, I. H. Abidi, H. Sims, K. Suenaga, S. T. Pantelides, and B. Özyilmaz, Nature (London) **577**, 199 (2020).

[7] G.-X. Chen, X.-G. Li, Y.-P. Wang, J. N. Fry, and H.-P. Cheng, Phys. Rev. B **95**, 045302 (2017).

[8] Y.-P. Wang and M.-Q. Long, Phys. Rev. B **101**, 024411 (2020).

[9] H. Lane, E. Pachoud, J. A. Rodriguez-Rivera, M. Songvilay, G. Xu, P. M. Gehring, J. P. Attfield, R. A. Ewings, and C. Stock, Phys. Rev. B **104**, L020411 (2021).

[10] B. Huang, G. Clark, E. Navarro-Moratalla, D. R. Klein, R. Cheng, K. L. Seyler, D. Zhong, E. Schmidgall, M. A. McGuire, D. H. Cobden, W. Yao, D. Xiao, P. Jarillo-Herrero, and X. D. Xu, Nature (London) **546**, 270 (2017).

[11] N. D. Mermin and H. Wagner, Phys. Rev. Lett. **17**, 1133 (1966).

[12] M. A. McGuire, H. Dixit, V. R. Cooper, and B. C. Sales, Chem. Mater. **27**, 612 (2015).

[13] S. Djurdjić-Mijin, A. Šolajić, J. Pešić, M. Šćepanović, Y. Liu, A. Baum, C. Petrovic, N. Lazarević, and Z. V. Popović, Phys. Rev. B **98**, 104307 (2018).

[14] Y. Liu and C. Petrovic, Phys. Rev. B **97**, 014420 (2018).

[15] J. F. Dillon Jr. and C. E. Olson, J. Appl. Phys. **36**, 1259 (1965).

[16] K. L. Seyler, D. Zhong, D. R. Klein, S. Y. Gao, X. O. Zhang, B. Huang, E. Navarro-Moratalla, L. Yang, D. H. Cobden, M. A. McGuire, W. Yao, D. Xiao, P. Jarillo-Herrero, and X. D. Xu, Nat. Phys. **14**, 277 (2018).

[17] Z. Wang, I. Gutiérrez-Lezama, N. Ubrig, M. Kroner, M. Gibertini, T. Taniguchi, K. Watanabe, A. Imamoğlu, E. Giannini, and A. F. Morpurgo, Nat. Commun. **9**, 2516 (2018).

[18] H. H. Kim, B. Yang, T. Patel, F. Sfigakis, C. Li, S. Tian, H. L. Lei, and A. W. Tsen, Nano Lett. **18**, 4885 (2018).

[19] B. Huang, G. Clark, D. R. Klein, D. MacNeill, E. NavarroMoratalla, K. L. Seyler, N. Wilson, M. A. McGuire, D. H. Cobden, D. Xiao, W. Yao, P. Jarillo-Herrero, and X. Xu, Nat. Nanotech. **13**, 544 (2018).

[20] S. Jiang, J. Shan, and K. F. Mak, Nature Mater. **17**, 406 (2018).

[21] T. Song, X. Cai, M. W.-Y. Tu, X. Zhang, B. Huang, N. P. Wilson, K. L. Seyler, L. Zhu, T. Taniguchi, K. Watanabe, M. A. McGuire, D. H. Cobden, D. Xiao, W. Yao, and X. Xu, Science **360**, 1214 (2018).

[22] D. R. Klein, D. MacNeill, J. L. Lado, D. Soriano, E. NavarroMoratalla, K. Watanabe, T. Taniguchi, S. Manni, P. Canfield, J. Fernández-Rossier, and P. Jarillo-Herrero, Science **360**, 1218 (2018).

[23] P. Jiang, C. Wang, D. Chen, Z. Zhong, Z. Yuan, Z.-Y. Lu, and W. Ji, Phys. Rev. B **99**, 144401 (2019).

[24] S. W. Jang, M. Y. Jeong, H. Yoon, S. Ryee, and M. J. Han, Phys. Rev. Materials **3**, 031001(R) (2019).

[25] N. Sivadas, S. Okamoto, X. Xu, C. J. Fennie, and D. Xiao, Nano Lett. **18**, 7658 (2018).

[26] J. Zhang, X. Cai, W. Xia, A. Liang, J. Huang, C. Wang, L. Yang, H. Yuan, Y. Chen, S. Zhang, Y. Guo, Z. Liu, and G. Li, Phys. Rev. Lett. **123**, 047203 (2019).

[27] H. Wang, V. Eyert, and U. Schwingenschlögl, J. Phys.: Condens. Matter **23**, 116003 (2011).

[28] O. Besbes, S. Nikolaev, N. Meskini, and I. Solovyev, Phys. Rev. B **99**, 104432 (2019).

[29] V. Kumar Gudelli and G.-Y. Guo, New J. Phys. **21**, 053012 (2019).

[30] W.-B. Zhang, Q. Qu, P. Zhu, and C.-H. Lam, J. Mater. Chem. C **3**, 12457 (2015).

[31] L. Craco, S. S. Carara, Y. C. Shao, Y. D. Chuang, and B. Freelon, Phys. Rev. B **102**, 195130 (2020).

[32] L. Craco, S. S. Carara, Y. C. Shao, Y. D. Chuang, and B. Freelon, Phys. Rev. B **103**, 235119 (2021).

[33] D. E. McNally, J. W. Simonson, K. W. Post, Z. P. Yin, M. Pezzoli, G. J. Smith, V. Leyva, C. Marques, L. DeBeer-Schmitt, A. I. Kolesnikov, Y. Zhao, J. W. Lynn, D. N. Basov, G. Kotliar, and M. C. Aronson, Phys. Rev. B **90**, 180403(R) (2014).

[34] G. Kotliar, S. Y. Savrasov, K. Haule, V. S. Oudovenko, O. Parcollet, and C. A. Marianetti, Rev. Mod. Phys. **78**, 865 (2006).

[35] K. Haule, C.-H. Yee, and K. Kim, Phys. Rev. B **81**, 195107 (2010).

[36] J. P. Perdew, K. Burke, and M. Ernzerhof, Phys. Rev. Lett **77**, 3865 (1996).

[37] P. Blaha, K. Schwarz, G. Madsen, D. Kvasnicka, and J. Luitz, WIEN2K, An Augmented Plane Wave + Local Orbitals Program for Calculating Crystal Properties (Karlheinz Schwarz, Techn. Universität Wien, Austria, 2001).

[38] K. Haule, Phys. Rev. Lett. **115**, 196403 (2015).

[39] See Supplemental Material at http://link.aps.org/supplemental/10.1103/PhysRevB.105.165127 for the dependences of charge gap and magnetic moment on U and J_H, band structure obtained with $U = 2\,\text{eV}$, $J_H = 0.7\,\text{eV}$, band structures obtained with the inclusion of spin-orbit coupling, detailed discussion about the origin of the strong valence fluctuations, as well as the formula describing the magnetic moment in terms of U and J_H.

[40] H. H. Kim, B. Yang, S. Li, S. Jiang, C. Jin, Z. Tao, G. Nichols, F. Sfigakis, S. Zhong, C. Li, S. Tian, D. G. Cory, G.-X. Miao, J. Shan, K. F. Mak, H. Lei, K. Sun, L. Zhao, and A. W. Tsen, Proc. Natl. Acad. Sci. USA **116**, 11131 (2019).
[41] Z. P. Yin, K. Haule, and G. Kotliar, Phys. Rev. B **86**, 195141 (2012).
[42] J. Mravlje, M. Aichhorn, T. Miyake, K. Haule, G. Kotliar, and A. Georges, Phys. Rev. Lett. **106**, 096401 (2011).
[43] K. Haule and G. Kotliar, New J. Phys. **11**, 025021 (2009).
[44] Z. P. Yin, K. Haule, and G. Kotliar, Nature Phys. **7**, 294 (2011).
[45] Z. P. Yin, K. Haule, and G. Kotliar, Nature Mater. **10**, 932 (2011).
[46] A. K. Kundu, Y. Liu, C. Petrovic, and T. Valla, Sci. Rep. **10**, 15602 (2020).
[47] X.-Y. Chen, M.-Q. Long, and Y.-P. Wang, Phys. Rev. B **102**, 214417 (2020).
[48] J. W. Simonson, Z. P. Yin, M. Pezzoli, J. Guo, J. Liu, K. Post, A. Efimenko, Z. Hu N.Hollmann, H.-J. Lin, C.-T. Chen, C. Marques, V. Leyva, G. Smith, J. W. Lynn, L. L. Sun, G. Kotliar, D. N. Basov, L. H. Tjeng, and M. C. Aronson, Proc. Natl. Acad. Sci. USA **109**, E1815 (2012).
[49] A. Narath, Phys. Rev. **140**, A854 (1965).
[50] A. Narath and H. L. Davis, Phys. Rev. **137**, A163 (1965).
[51] H. L. Davis and A. Narath, Phys. Rev. **134**, A433 (1964).
[52] E. J. Samuelsen, R. Silberglit, G. Shirane, and J. P. Remeika, Phys. Rev. B **3**, 157 (1971).
[53] Z. Cai, S. Bao, Z.-L. Gu, Y.-P. Gao, Z. Ma, Y. Shangguan, W. Si, Z.-Y. Dong, W. Wang, Y. Wu, D. Lin, J. Wang, K. Ran, S. Li, D. Adroja, X. Xi, S.-L. Yu, X. Wu, J.-X. Li, and J. Wen, Phys. Rev. B **104**, L020402 (2021).
[54] B. Morosin and A. Narath, J. Chem. Phys. **40**, 1958 (1964).
[55] L. L. Handy and N. W. Gregory, J. Am. Chem. Soc. **74**, 891 (1952).
[56] G. Kresse and J. Furthmüller, Comput. Mater. Sci. **6**, 15 (1996).